TENTH AUSTRALASIAN FLUID MECHANICS
CONFERENCE - UNIVERSITY OF MELBOURNE
11-15 DECEMBER 1989

TRANSONIC VISCOUS FLOW COMPUTATIONS ABOUT A COMPLETE AIRCRAFT USING THE NAVIER-STOKES EQUATIONS

Neal. M. CHADERJIAN and Jolen FLORES

NASA Ames Research Center
Moffett Field, California 94035
USA

ABSTRACT

A numerical approach for simulating the viscous transonic flow about the complete F-16A fighter aircraft is presented using the Navier-Stokes equations. This finite difference approach utilizes a body conforming zonal grid system to provide appropriate viscous clustering near all body surfaces. A comparison between computational and experimental pressure coefficients is good, and integrated quantities such as lift and drag are within 2.6% and 1.6% respectively. The versatility of the method is demonstrated by further modeling the flow inside the inlet up to the compressor face and the exhaust nozzle plume. Results for the F-16A in sideslip are also presented and indicate the proper trends.

INTRODUCTION

The traditional approach to aircraft design relies heavily upon experimental data to aid the engineer in the design process, however, this approach is not without certain drawbacks. For example, it can be very expensive and time consuming to fabricate and test a wind-tunnel model. Moreover, wind-tunnel wall effects, instrument interference, and unrealistic flight conditions can also affect the validity and accuracy of experimental data. It has been anticipated that computational fluid dynamics (CFD) can help alleviate some of these difficulties and provide additional information to the design engineer that would compliment experimental data.

In order to address this need, several Euler solutions about complete aircraft have recently appeared in the literature, e.g., Karman et al (1986), Eberle (1986), and Jameson & Baker (1987). The main goal of this research is to develop a CFD approach for simulating viscous flow about a realistic aircraft geometry and verify it by comparing a benchmark computation with experimental data.

In order to accomplish this goal, the Transonic Navier-Stokes code (TNS) has been developed and applied to the F-16A fighter geometry. This particular geometry was chosen because of its complex shape and available experimental data. The complexity of the F16-A geometry is readily seen in Fig. 1. It would be difficult, if not impossible, to adequately resolve the viscous flow physics near all body surfaces with a single grid. A zonal grid approach has therefore been adopted which partitions the physical space into an ensemble of simple geometric shapes. This reduces the difficulty of grid generation to a manageable problem and provides a straight forward method of local grid refinement.

In the following sections, a brief description of the method will be presented, then a discussion of results, and finally some concluding remarks will be made.

NUMERICAL APPROACH

The TNS code uses an implicit, approximately factored, diagonal, central-difference algorithm due to Pulliam & Chaussee (1981) for integrating the time-accurate, Reynolds-averaged, Navier-Stokes equations. These equations are solved in strong conservation-law form with body conforming coordinates. The latter simplifies the application of boundary conditions. Explicit and implicit numerical dissipation (second- and fourth-order) is added to damp out high-frequency errors due to high gradients, e.g., shocks. Local time stepping based on the transformation Jacobian is used to accelerate this time-accurate formulation to a steady state. An algebraic eddy viscosity model due to Baldwin & Lomax (1978) is used to model turbulence.

A zonal grid procedure is utilized to simplify the grid generation process and provide for local grid refinement in a straight forward maner. For example, Fig. 2 shows a cross-sectional view of the F16-A wing/fuselage zonal topology. Zones near the aircraft body have a high degree of clustering normal to the body to capture the viscous effects of the boundary layer. The thin-layer, Reynolds-averaged, Navier-Stokes equations are solved in these zones. For zones with viscous effects in two directions, e.g., the wing/fuselage juncture zone, the thin-layer approximation is applied in two directions. Thus cross-derivative terms are neglected. The Euler equations are applied in zones farther away from the body where viscous effects are negligible. These zones have coarser grid spacing appropriate for inviscid flow.

The zonal grids are carefully (but automatically) constructed to overlap by a specific number of cells, usually one or two relative to the coarse grid, so that the outer boundary of one zone is coincident with an interior surface of another zone. Zonal boundary conditions are imposed by interpolating the flow variables from the interior of one zone onto the boundary of another zone. When flow conservation across zonal boundaries is important, e.g., a shock extending from one zone into another, the interface between the zones have coincident grid points. In this case, the interpolation reduces to direct injection and conservation is maintained.

Figure 3 shows the zonal topology at the inlet face. The diverter region is divided into two zones, one directly below the fuselage and one directly above the inlet. A zone extends from the inlet face upwind and blends into the underside of the fuselage. Extrapolation conditions at the inlet face are used to model flow-through conditions, or additional zones are created inside the inlet to model flow with spillage.

The flow solution is advanced from iteration level n to $n+1$ one zone at a time. First, the zonal boundary conditions are applied. This includes physical boundary conditions as well as zonal interface conditions, where the most recent data available is used. The flow solver then updates values interior to the zone. Once all zones have been updated, the code proceeds to the next iteration level. This process is repeated until convergence is achieved. A more complete description of the TNS code, the numerical algorithm, and the zonal interfacing procedure is described by Flores & Chaderjian (1988).

RESULTS

All of the computations described below correspond to a freestream Mach number $M_\infty = 0.90$, angle of attack $\alpha = 6.0°$, and a Reynolds number based on the wing root chord $Re = 4.5 \times 10^6$. The experimental wind-tunnel data used for comparison purposes is reported by Reue et al (1976).

Zero Yaw

The first case corresponds to the F16-A mounted on a sting, which is similar to the wind-tunnel model. Twenty

seven zones totaling 528,000 grid points provide adequate resolution to model the problem. A single zone with the same number of grid points would not give the same level of accuracy because an excessive number of grid points would be used in the far field rather than near the body. The average y^+ one grid point off the body was 3. Symmetry plane boundary conditions are imposed along the fuselage centerline. The wind-tunnel walls are not modeled.

A comparison between computational and experimental pressure coefficients (C_p) for the wing and fuselage centerline are shown in Fig. 4. Overall the comparison is good, and the double shock pattern on the wing is predicted. The expansion spike near the wing leading edge is due to inadequate grid resolution of the leading edge nose radius, which is very small for fighter aircraft wings. A Mach number correction $\Delta M = 0.02$ is used to account for wind-tunnel wall effects. Initially, computed shock positions were uniformly upstream of the experimental ones along the entire wing. Reue et al (1976) did not give adequate information to determine the test-section influence on free-flight conditions; however, the uniform improvement along the wing due to the Mach number correction suggests that there is some influence from the wind-tunnel walls. The comparison of C_p along the fuselage centerline is also good. A weak shock on the canopy is predicted. There is a slight disagreement downwind of the vertical tail because the gap between the fuselage and vertical tail was not modeled in the grid.

One of the most challenging aspects of the F16-A geometry is modeling the engine inlet and diverter channel. A comparison between computation and experimental C_p is shown in Fig. 5. The normalized streamwise coordinate ξ is zero at the inlet face and one at the diverter exit where the diverter merges into the fuselage. The comparison is good, with a slight underprediction of C_p at the cross-section station $\xi = 0.37$. This is attributed to flow though inlet conditions imposed in the computational model while the experimental model had a slight amount of spillage. Notice the comparison at $\xi = 0.67$ is improved. At this downwind position the spillage has a nominal effect. The comparison of computational and experimental C_p on the horizontal and vertical tails is also shown in Fig. 5. The left side of each graph corresponds to the leading edge of the control surface and the right side to the trailing edge. There is a slightly greater expansion on these surfaces in the computations (with the wing Mach number correction) than indicated in the experiment. This is to be expected since the Mach number correction for the empennage would be less than that required for the wing due to its reduced span.

Figures 6 and 7 indicate pressure contours on the upper and lower portions of the aircraft body respectively. The double shock pattern on the wing, the compression on the canopy forebody, and the general complexity of the flow near the inlet is evident.

The computed C_L underpredicted the experimental value by 2.6% while C_D overpredicted the experimental value by 1.6%. Overall, the comparisons are good; but more grid refinement is indicated, especially near the wing leading edge. This case took approximately 5000 iterations to reduce the L_2-norm of the residual in all zones by at least three orders of magnitude. This required about 25 hours of CPU time on the Cray XM-P supercomputer. Due to the developmental nature of this first solution, smaller time steps were used than were optimum. It is expected that the CPU time can be reduce to about 1 hours.

In order to demonstrate the versatility of the zonal approach, additional zones were added inside the inlet up to the compressor face, and downwind of the exhaust nozzle to model the exhaust plume. There are now 31 zones with a total of 551,000 grid points. Figure 8 indicates the temperature contours aft of the exhaust nozzle along the symmetry plane. A nozzle exit to freestream pressure ratio of 2 was specified, as well as a nozzle exit to freestream temperature ratio of 5. The nozzle exit plane Mach number was specified to be 1. At Mach numbers near 1, the characteristics formed are essentially vertical expansion waves. (This is evident by the coalescence of contour levels near the exhaust nozzle exit plane). Downwind of the expansion fan, a compression wave system develops due to the reflection of characteristics off the plume boundary. The lower plume boundary is slightly displaced due to angle of attack effects.

Yaw Case

Computations are also presented for the F16-A with sideslip of $\beta = 5.0°$. The 27 zone grid system is reflected about the symmetry plane. This resulted in 54 zones and a total of 1.1×10^6 grid points. Figure 9 indicates the pressure contours on the top portion of the aircraft. The freestream air is approaching the fuselage from the right side (when facing the aircraft). The different positions of the leading edge wing shocks on the windward and leeward sides as well as the shift of pressure contours along the centerline of the aircraft indicate the effects of sideslip. The lift of the windward wing is greater than the leeward wing, as expected, due to the different "effective" sweep angles.

Figure 10 shows computational particle traces which are released at a cross-sectional location just downwind of the nose. The particle traces released from the leeward side are displaced by the canopy and proceed along the fuselage past the leeward side of the vertical tail. The particle traces released from the windward side are also displaced by the canopy, however, some cross over the fuselage centerline and proceed along the leeward side of the vertical tail while others proceed along the windward side.

Computational particle traces released near the leading edge and tip of the vertical tail are shown in Fig. 11. The formation of the tip vortex is evident. Traces beginning near the leading edge converge along a separation line, and eventually roll up into the tip vortex. Particles which are released further upstream of the leading edge proceed in a quasi two-dimensional manner and then move slightly outboard due to a spanwise pressure gradient.

CONCLUSIONS

Steady transonic viscous flow computations about the complete F16-A fighter aircraft have been presented using the thin-layer, Reynolds-averaged, Navier-Stokes equations and a zonal grid approach. The viability and accuracy of the zonal approach was demonstrated by a bench mark computation, for freestream conditions of $M_\infty = 0.9$, $\alpha = 6.0°$, and $Re = 4.5 \times 10^6$. A comparison of computational and experimental pressure coefficients was generally good on all body surfaces, and the lift and drag coefficients were within 2.6% and 1.6%, respectively. The versatility of the zonal approach was demonstrated by later adding zones inside the inlet up to the compressor face and downwind of the exhaust nozzle to model the exhaust plume. Computations were also presented for the F-16A with five degrees of sideslip and indicate the proper trends. As super computer speed, memory, and availability continue to improve, industry can begin the task of using Navier-Stokes codes to help evaluate realistic aircraft configurations.

REFERENCES

Baldwin, B.S., and Lomax, H.(1978) Thin Layer Approximation and Algebraic Model for Separated Turbulent Flow. AIAA Paper No. 78-257.

Eberle, A. (1986). Euler Solution for a Complete Fighter Aircraft Configuration at Sub- and Supersonic Speed. AGARD Paper No. 17, April.

Flores, J., and Chaderjian, N.M. (1988) A Zonal Navier -Stokes Methodology For Flow Simulation About A Complete Aircraft. AIAA Paper No. 88-2506, and to appear in the AIAA Journal of Aircraft.

Jameson, A., and Baker, T.J. (1987). Improvements to the Aircraft Euler Method. AIAA Paper 87-0452.

Karman, S.L., Steinbrenner, J.P., and Kisielewski, K. M. (1986). Analysis of the F-16 Flow Field by a Block Grid Euler Approach. AGARD Paper No. 18, April.

Pulliam, T. H. and Chaussee, D. S.(1981) A Diagonal Form of An Implicit Approximate-Factorization Algorithm. In the Journal of Computational Physics, Vol. 39, No. 2, 1981, pp. 347-363.

Reue, G. L., Doberenz, M. E., and Wilkins, D. D. (1976) Component Aerodynamic Load from 1/9-Scale F-16A Loads Model. In the General Dynamics Report 16PR316, Fort Worth, Texas.

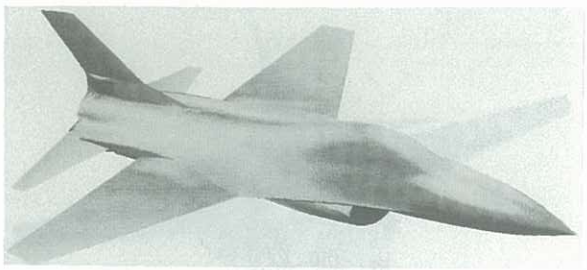

Fig. 1 Surface geometry of the F-16A.

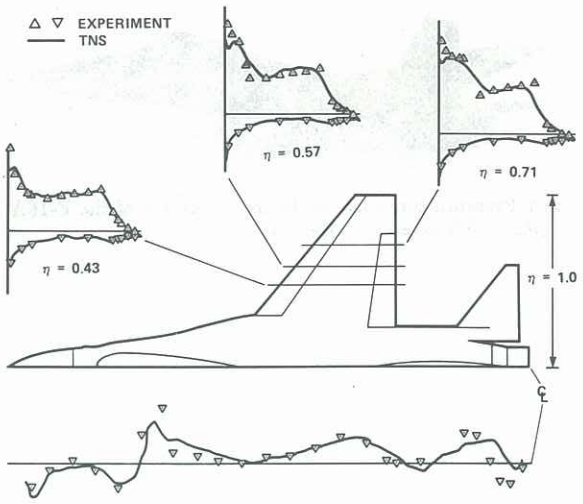

Fig. 4 Comparison of computational and experimental pressure coefficients on the wing and along the centerline of the fuselage for $M_\infty = 0.9$, $\alpha = 6.0°$, $Re = 4.5 \times 10^6$.

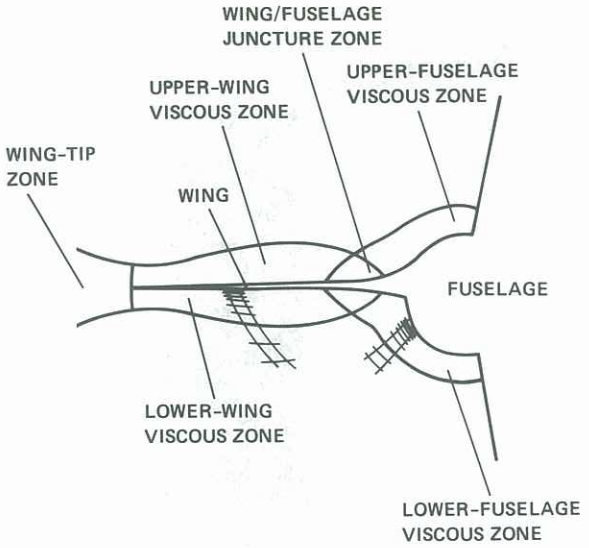

Fig. 2 Zonal grid topology at a fuselage/wing cross-section.

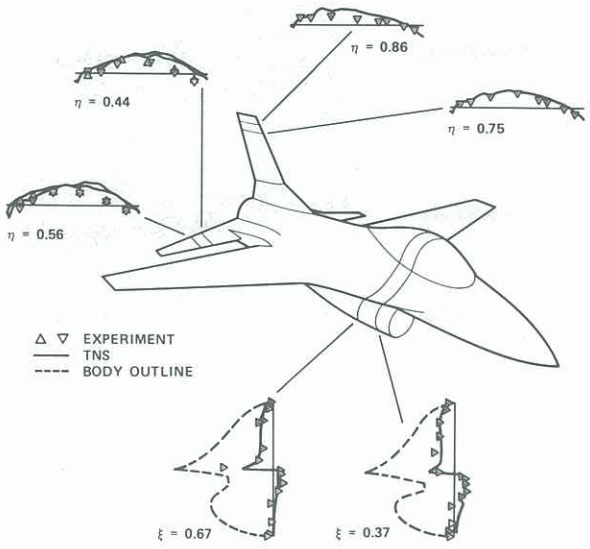

Fig. 5 Comparison of computational and experimental pressure coefficients on the horizontal and vertical tails and two cross-section stations through the inlet/diverter region $M_\infty = 0.9$, $\alpha = 6.0°$, $Re = 4.5 \times 10^6$.

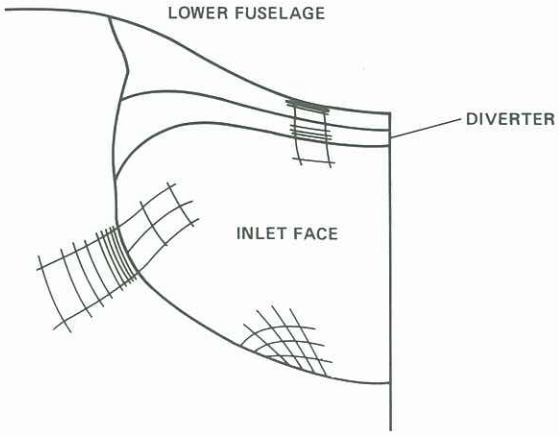

Fig. 3 Zonal grid topology at the inlet face.

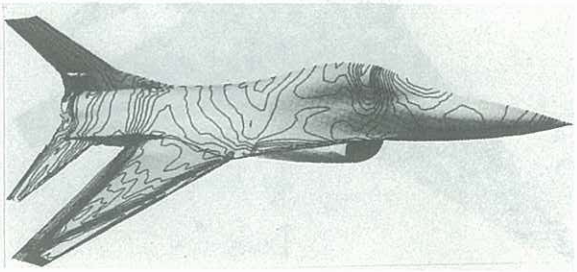

Fig. 6 Pressure contours on the upper surface of the F-16A for $M_\infty = 0.9$, $\alpha = 6.0°$, $Re = 4.5 \times 10^6$.

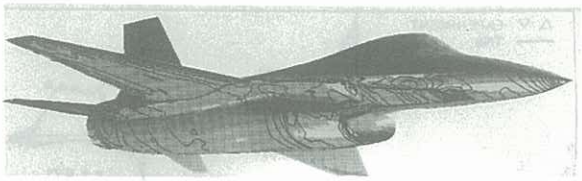

Fig. 7 Pressure contours on the lower surface of the F-16A for $M_\infty = 0.9$, $\alpha = 6.0°$, $Re = 4.5 \times 10^6$.

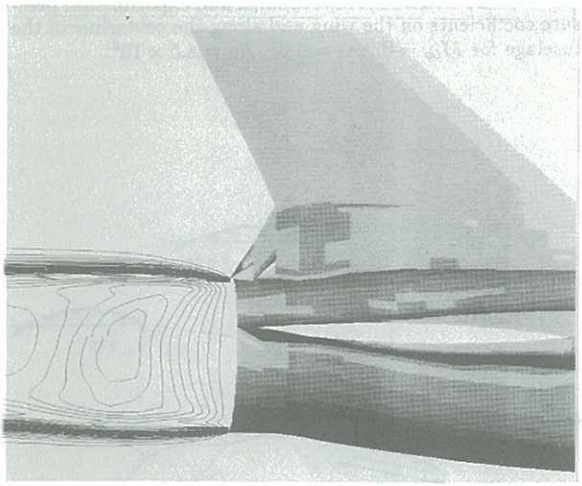

Fig. 8 Computed temperature contours on the symmetry plane of the exhaust plume for $M_\infty = 0.9$, $\alpha = 6.0°$, $Re = 4.5 \times 10^6$.

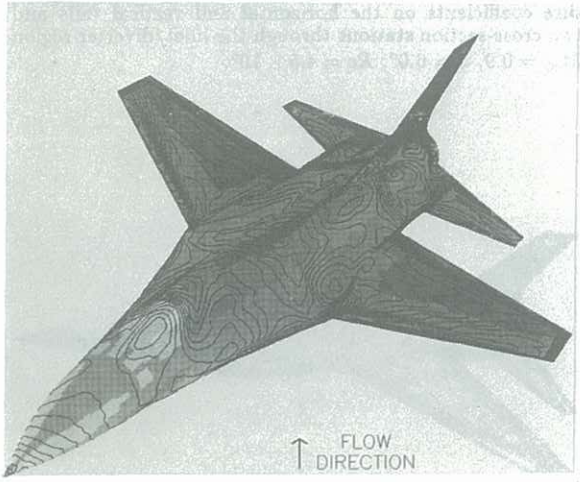

Fig. 9 Computed pressure contours on the upper surface of the F-16A in sideslip for $M_\infty = 0.9$, $\alpha = 6.0°$, $\beta = 5.0°$, $Re = 4.5 \times 10^6$.

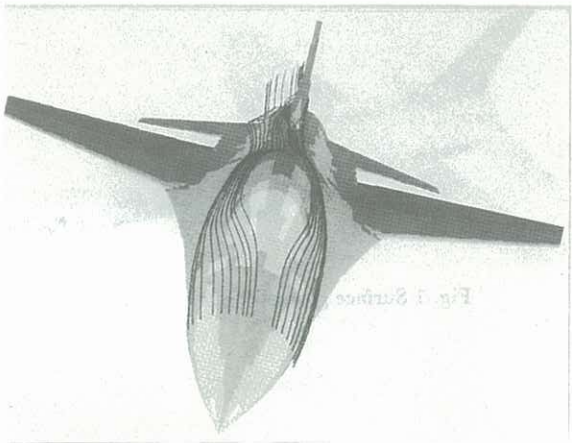

Fig. 10 Computed particle traces for the F-16A in sideslip with $M_\infty = 0.9$, $\alpha = 6.0°$, $\beta = 5.0°$, $Re = 4.5 \times 10^6$.

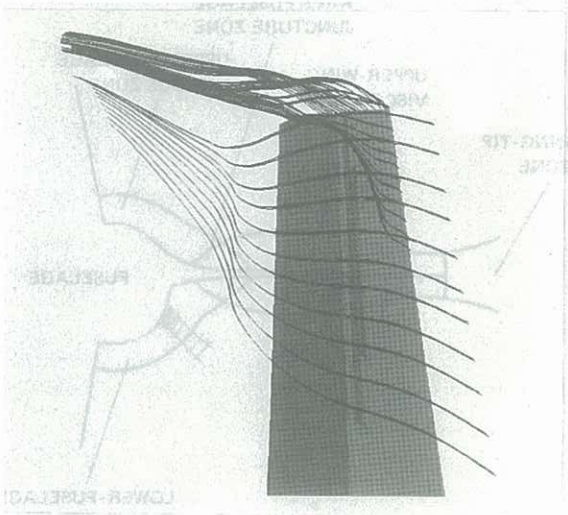

Fig. 11 Computed particle traces for the vertical tail with $M_\infty = 0.9$, $\alpha = 6.0°$, $\beta = 5.0°$, $Re = 4.5 \times 10^6$.